Available online at www.sciencedirect.com

ScienceDirect

Thin Solid Films 517 (2008) 1032 – 1036

www.elsevier.com/locate/tsf

Effect of Sn-doped on microstructural and optical properties of ZnO thin films deposited by sol–gel method

Chien-Yie Tsay [a,*], Hua-Chi Cheng [b], Yen-Ting Tung [a], Wei-Hsing Tuan [c], Chung-Kwei Lin [a]

[a] Department of Materials Science and Engineering, Feng Chia University, Taichung 407, Taiwan, ROC
[b] Department of Materials Science and Engineering, National Chiao Tung University, Hsinchu 300, Taiwan, ROC
[c] Department of Materials Science and Engineering, National Taiwan University, Taipei 106, Taiwan, ROC

Available online 15 June 2008

Abstract

In this study, transparent thin films of Sn-doped ZnO (ZnO:Sn) were deposited onto alkali-free glass substrates by a sol–gel method; the effect of Sn doping on crystallinity, microstructural and optical properties was investigated. The atomic percentages of dopant in ZnO-based sols were Sn/Zn = 0, 1, 2, 3, and 5 at.%. The as-deposited films were pre-heated at 300 °C for 10 min and then annealed in air at 500 °C for 1 h. The results show that Sn-doped ZnO thin films demonstrate obviously improved surface roughness, enhanced transmittance in the 400–600 nm wavelength range and reduced average crystallite size. Among all of the annealed ZnO-based films in this study, films doped with 2 at.% Sn concentration exhibited the best properties, namely an average transmittance of 90%, an RMS roughness value of 1.92 nm and a resistivity of 9.3×10^2 Ω-cm.
© 2008 Elsevier B.V. All rights reserved.

Keywords: Transparent oxide semiconductors; ZnO thin films; Sn doping; Sol–gel method

1. Introduction

Wide bandgap (>3 eV) transparent oxides have been extensively used for photovoltaic devices and optical–electrical devices. Among these materials, zinc oxide (ZnO) is a promising candidate for novel device applications, such as transparent electronics [1–3] and flexible displays [4,5]. ZnO exhibits non-toxicity, high transparency, a wide range of conductivity from metallic to insulating, and high crystallinity. Its unique electrical and optical properties have made it popular in piezoelectric transducers, surface acoustic wave (SAW) devices, laser diodes, photoconductive UV detectors and gas sensors, etc. Recently, interest in ZnO-based thin films has focused on flat-panel displays (FPDs) and photovoltaic applications, such as the anodic electrode of organic light-emitting device (OLED) displays [6,7], the active channel layer of thin-film transistors (TFTs) [8–10] and the transparent electrode/window layer of thin-film solar cells [11,12].

ZnO is an n-type oxide semiconductor material with a direct wide bandgap of 3.3 eV. Its electrical characteristics can be controlled by doping with ternary elements or adjusted process conditions [13,14]. The carrier mobility of the pure ZnO exceeds the field effect mobility of hydrogenated amorphous silicon (a-Si:H), which serves as the active channel layer in typical TFT arrays. In addition, polycrystalline ZnO films can be prepared in a normal atmosphere and possess low photosensitivity. Therefore, ZnO may replace a-Si:H as an active layer; for this reason, the subject presently attracts much attention.

ZnO-based thin films have been prepared by various thin-film deposition techniques, such as RF/DC magnetic sputtering deposition, pulsed laser deposition, chemical vapor deposition, chemical bath deposition, spray pyrolysis, sol–gel method, etc. The solution-based process offers a simple, low cost and large area thin-film coating method as an alternative to vacuum deposition techniques (PVD or CVD). Use of the solution process to form oxide semiconductors may improve the manufacturing throughput of microelectrical devices since it enables maskless processes, including inkjet printing [15] and selective electroless plating [16], etc. The sol–gel method is one of the common solution processes; it is popularly used for polycrystalline oxide thin-film deposition [17,18]. ZnO-based semiconductor films have served as active channel layers in

* Corresponding author. Tel.: +886 4 24517250x5312; fax: +886 4 24510014.
E-mail address: cytsay@fcu.edu.tw (C.-Y. Tsay).

0040-6090/$ - see front matter © 2008 Elsevier B.V. All rights reserved.
doi:10.1016/j.tsf.2008.06.030

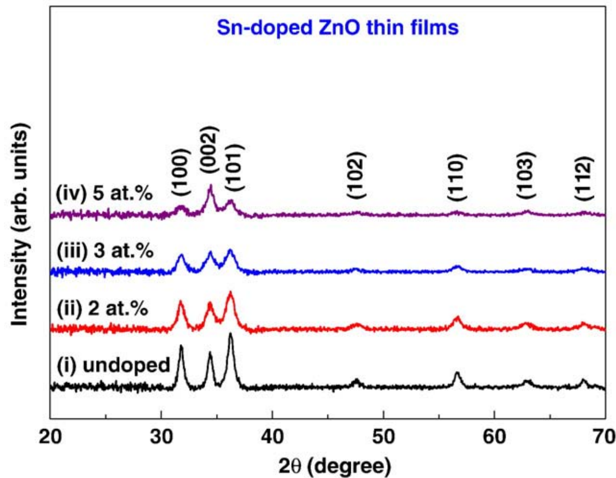

Fig. 1. X-ray diffraction patterns of undoped and Sn-doped ZnO thin films annealed at 500 °C for 1 h.

TFTs. Kwon et al. [19] have indicated that controlling the carrier density of the active layer is a challenge in ZnO-based TFTs, since the active layer supplies high carrier density that will conduct when an applied gate voltage is absent.

Lee et al. [20] have reported on TFTs with spin-coated $Zn_{1-x}Zr_xO$ thin films (ZnO doped with a group IV group element) as active channel layers. However, transparent oxide semiconductors of Sn-doped ZnO thin films prepared by a solution-based process or a vacuum deposition technique have not been reported. The ionic radius of Sn^{4+} (0.69 Å) is smaller than Zn^{2+} (0.74 Å), and thus Sn^{4+} ions can replace Zn^{2+} ions in substitutional sites [13]. The present study used a sol–gel method to prepare transparent oxide semiconductors with Sn-doped ZnO thin films; it investigated the effects of Sn concentration on crystallinity, microstructure and optical properties.

2. Experimental

Sn-doped ZnO (ZnO:Sn) thin films were prepared on glass substrates by a sol–gel method. Zinc acetate dehydrate (Zn $(CH_3COO)_2{\cdot}2H_2O$) and tin tetrachloride ($SnCl_4$) were dissolved in 2-methoxyethanol, and then monoethanolamine (MEA) was added to the solution as a stabilizer. The concentration of metal ions in ZnO:Sn sols was controlled at 0.35 M and Sn/Zn ratios varied from 0 to 5 at.%. Each complex solution was stirred for 2 h at 60 °C until a transparent and homogenous sol was obtained. All ZnO:Sn gel films were coated onto alkali-free glass (Corning 1737, with dimension 5×5 cm^2) using spin coating at a speed of 1000 rpm for 30 s. These as-coated films were pre-heated at 300 °C for 10 min immediately after coating. After repeating the coating procedure three times, the films were annealed in air at 500 °C for 1 h.

The crystallinity levels of Sn-doped ZnO thin films after annealing were determined by glancing angle X-ray diffraction (GAXRD). These diffracted patterns were examined on a MAC Science MAXP3 diffractometer with a glancing incident angle of 1°. Surface morphology and microstructure of each ZnO:Sn film were observed using a field-emission scanning electron microscope (FE-SEM, HITACHI S-4800, Japan). A scanning probe microscope (SPM, Digital Instrument NS4/D3100CL, Germany) was used to analyze the films' surface roughness levels. The resistivities were measured at room temperature by a high resistivity meter (MCP-HT450, DIA INSTRUMENTS CO., LTD, Japan). A spectrophotometer (Mini-D2T, Ocean Optics Inc., USA) was used to measure optical transmittance spectra in the visible ranges of these films.

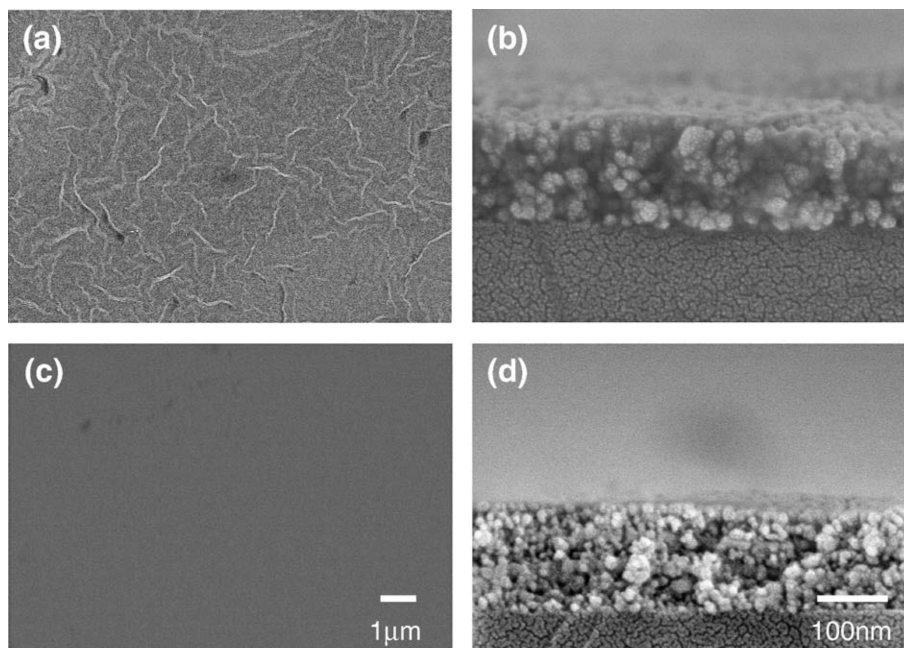

Fig. 2. SEM micrographs of plane view and cross-section of Sn-doped ZnO thin films: (a), (b) undoped sample and (c), (d) 2 at.% Sn-doped sample.

3. Results and discussion

X-ray diffraction patterns of undoped ZnO and Sn-doped ZnO films are presented in Fig. 1. These patterns correspond to three main diffraction peaks of crystallized ZnO, namely (100), (002) and (101). This result revealed the as-prepared films had been annealed at 500 °C for 1 h, and had given polycrystalline films with a hexagonal wurtzite structure (Zincite, JCPDS 36-1451). These diffractographs show that the intensities of diffraction peaks declined as Sn concentrations increased, i.e. Sn doping within ZnO films caused the crystallinity to degenerate. Moreover, the XRD patterns of the ZnO:Sn films that were prepared without the formation of a secondary phase, such as SnO_2 and the 5 at.% Sn-doped ZnO thin film (curve (iv) in Fig. 1), show high (002) peak intensities; this indicates such films exhibit *c*-axis preferred orientation.

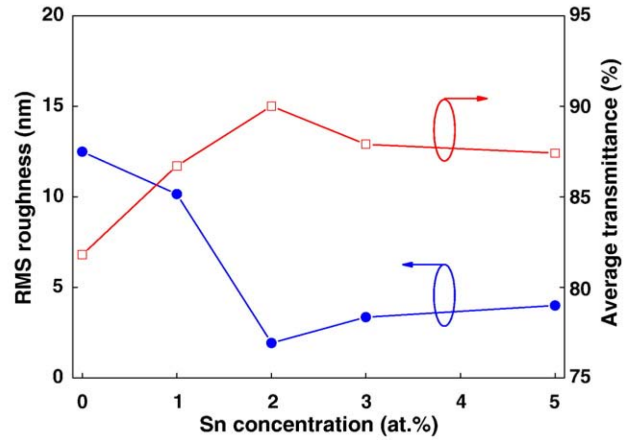

Fig. 4. Surface roughness and average transmittance of ZnO:Sn thin films as a function of Sn concentration.

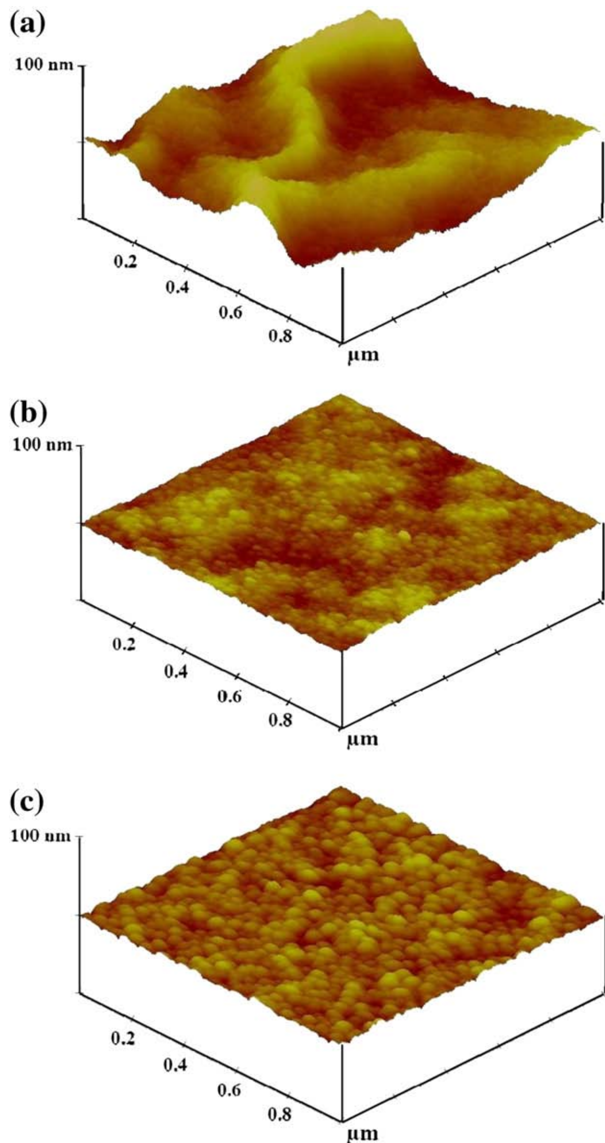

Fig. 3. SPM images of Sn-doped ZnO thin films: (a) undoped sample, (b) 2 at.% and (c) 5 at.% Sn-doped samples.

In addition, increased Sn concentrations slightly shift the position of (002) peaks to higher diffraction angles. Park et al. [21] have reported that the (002) peak shift to a high angle is because dopant ions have smaller radii than Zn^{2+} ions and dopant ions only substituted for Zn^{2+} ions. The average crystallite size (*d*) of these samples was estimated using Scherrer's formula [22]:

$$d = \frac{0.9\lambda}{B\cos\theta_{\mathrm{B}}},$$

where λ is the X-ray wavelength of 1.54 Å, θ_{B} is the Bragg diffraction angle and B is the FWHM (full width at half maximum) of θ_{B}. The calculated average crystallite sizes of undoped and 1 at.% Sn-doped ZnO thin films were 13.0 and 10.0 nm, respectively. When the Sn concentration increased from 2 to 5 at.%, the average crystallite size decreased about 8.2–8.8 nm.

Spin-coating method is a simple and cheap oxide thin-film deposition technique, but it requires soluble reagents. It is possible to control the film thickness by merely adjusting the solution viscosity or coating times. The plane view of an SEM micrograph of an annealed undoped ZnO film shows fiber-like streaks or wrinkles (Fig. 2(a)). However, the doped samples do not display that appearance, as can be seen from the surface micrograph of 2 at.% Sn-doped ZnO film (Fig. 2(c)). According to a previous report [23], the fiber-like streaks or wrinkles were induced by the shortness of OH and OR groups. Thus, a relatively smooth surface will be obtained when starting materials can provide enough OH and OR groups. Cross-sectional SEM micrographs of the undoped and 2 at.% Sn-doped ZnO thin films are shown in Fig. 2(b) and (d), respectively. Fig. 2(b) is an SEM micrograph of undoped ZnO thin film that shows its average thickness to be about 150 nm. Fig. 2(d) shows that the average thickness of doped films is approximately 150 nm and Sn doping in ZnO films obviously improves the surface flatness and enhances the uniformity of film thickness. This SEM micrograph (Fig. 2(d)) also reveals that Sn doping ZnO films can reduce the average crystallite size; that result agrees with XRD measurements.

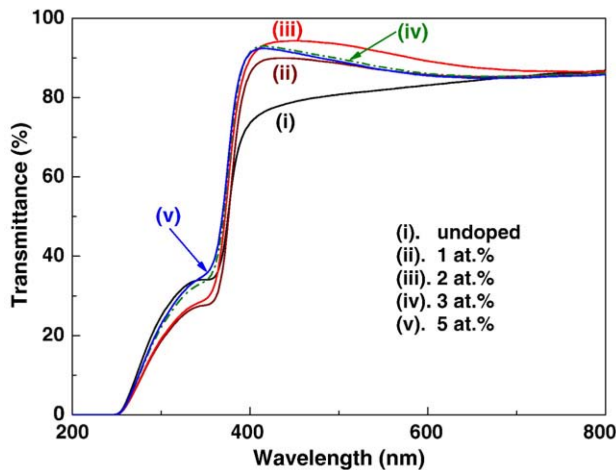

Fig. 5. Optical transmittance spectra of undoped ZnO and Sn-doped ZnO thin films.

SPM images of the ZnO:Sn thin films are shown in Fig. 3. These images show that the surface morphologies of the films were strongly dependent on the dopant concentration. In addition, it is apparent that the reduction of surface roughness results from a decrease in the average crystallite size in the ZnO films after Sn substitution. The plot of surface roughness levels of ZnO:Sn thin films as a function of Sn concentrations is shown in Fig. 4. A significant improvement of surface roughness with Sn doping can be noticed. The root-mean-square (RMS) roughness decreased with Sn concentrations of up to 2 at.% but increased with concentrations greater than that (Fig. 4). That is, the 2 at.% Sn-doped ZnO thin films exhibited the smallest RMS value (1.92 nm) among all of the annealed ZnO:Sn thin films investigated in this study. Fig. 3(c) shows the 5 at.% doped films had different particle sizes that caused them to exhibit higher RMS roughness compared with the 2 at.% doped ZnO thin films.

ZnO exhibits a wide range of conductivity; its behavior varies from metallic to insulating. Its electrical characteristics can be controlled by doping with ternary elements or by adjusting process conditions. The resistivities of undoped and doped films were measured at room temperature by using a high resistivity meter. Experimental results show that an undoped film exhibits a resistivity of 2.4×10^2 Ω-cm and the resistivities of 1, 2 and 5 at.% Sn-doped ZnO thin films were 3.4×10^2, 9.3×10^2 and 9.0×10^2 Ω-cm, i.e. when the Sn concentration increased from 2 to 5 at.%, the resistivity of film scarcely changed. The resistivity of doped films increased with increasing dopant concentration, which may be due to a decrease in carrier concentration caused by carrier traps at the grain boundaries [13].

Fig. 5 shows the optical transmittance spectra with wavelengths from 200 to 800 nm for the undoped and Sn-doped ZnO thin films. From this figure, all samples show sharp absorption edges in the UV region and these absorption edges slightly shifted to shorter wavelengths (blueshift) when Sn dopant was present within the ZnO thin films. The bandgaps of ZnO:Sn thin films were calculated from transmittance spectra by applying the Tauc mode [24]. In this present study, the bandgaps increased from 3.23 to 3.27 eV as the Sn dopants increased from 0 to 5 at.%. Tan et al. have indicated that the optical bandgap blueshift is due to the poor crystallinity of ZnO films [25].

The average optical transmittance in the visible range for undoped ZnO films was about 81.8% and they exhibited an absorption edge at a wavelength of about 360 nm (curve (i) in Fig. 5). Fig. 5 also shows that Sn-doped samples had higher transparency than undoped ZnO samples. However, the average transmittances of doped films with 3 and 5 at.% were lower than that of 2 at.% films (Fig. 4). This result is in good agreement with the measurements of surface roughness. Lee et al. [13] have indicated that the lower transmittance in Sn-doped ZnO films may be due to the increase in optical scattering caused by rough surface morphology. In this study, the 2 at.% Sn-doped ZnO thin film exhibited 90% average transparency, which was the best transparency among doped samples and gave an increase of about 10% over the undoped ZnO film. Such a transparent oxide semiconductor (TOS) film has a potential application as an active channel layer for transparent thin-film transistors (TTFTs).

4. Conclusions

Transparent oxide semiconductor thin films of tin-doped zinc oxide have been successfully prepared onto alkali-free glass by the sol–gel method. The as-deposited films were annealed in air at 500 °C for 1 h. The results show that Sn doping in ZnO thin films markedly decreased the surface roughness, improved transparency in visible range, and gave a finer microstructure than that of undoped ZnO thin films. Moreover, ZnO thin film doped with 5 at.% Sn concentration exhibited preferred orientation along the (002) plane. The energy bandgap of ZnO:Sn thin films was about 3.23–3.27 eV. Among the ZnO:Sn thin films investigated in the present study, the 2 at.% Sn-doped ZnO thin film exhibited the smoothest surface morphology, the best average transparency of 90% and the highest resistivity of 9.3×10^2 Ω-cm.

Acknowledgments

The authors gratefully acknowledge the financial support by the National Science Council of Republic of China under Contract No. NSC 96-2221-E-035-055-MY3 and Taiwan TFT-LCD Association (TTLA) under Contract No. A643TT1000-S21.

References

[1] H. Hosono, Thin Solid Films 515 (2007) 6000.
[2] A. Pimentel, E. Fortunato, A. Gonçalves, A. Marques, H. Águas, L. Pereira, I. Ferreira, R. Martins, Thin Solid Films 487 (2005) 212.
[3] J.F. Wager, Science 300 (2003) 1245.
[4] K. Nomura, A. Takagi, T. Kamiya, H. Ohta, M. Hirano, H. Hosong, Jpn. J. Appl. Phys. 45 (2006) 4303.
[5] I.D. Kim, Y.W. Choi, H.L. Tuller, Appl. Phys. Lett. 87 (2005) 043509.
[6] Y.R. Park, E. Nam, Y.S. Kim, Jpn. J. Appl. Phys. 47 (2008) 468.
[7] D. Xu, Z. Deng, Y. Xu, J. Xiao, C. Liang, Z. Pei, C. Sun, Phys. Lett., A 346 (2005) 148.
[8] C.G. Choi, S.J. Seo, B.S. Bae, Electrochem. Solid-State Lett. 11 (2008) H7.

[9] B.S. Ong, C. Li, Y. Li, Y. Wu, R. Loutfy, J. Am. Chem. Soc. 129 (2007) 2750.
[10] Y.J. Chang, D.H. Lee, G.S. Herman, C.H. Chang, Electrochem. Solid-State Lett. 10 (2007) H135.
[11] F. Ruske, C. Jacobs, V. Sittinger, B. Szyszka, W. Werner, Thin Solid Films 515 (2007) 8695.
[12] H. Tanaka, T. Shimakawa, T. Miyata, H. Sato, T. Minami, Appl. Surf. Sci. 244 (2005) 568.
[13] J.H. Lee, B.O. Park, Thin Solid Films 426 (2003) 94.
[14] Y.S. Kim, W.P. Tai, S.J. Shu, Thin Solid Films 491 (2005) 153.
[15] D.H. Lee, Y.J. Chang, W. Stickle, C.-H. Chang, Electrochem. Solid-State Lett. 10 (2007) K51.
[16] C.Y. Tsay, C.K. Lin, H.M. Lin, S.C. Chang, B.C. Chung, Mater. Sci. Forum 561–565 (2007) 1165.
[17] A.M.P. Santos, E.J.P. Santos, Mater. Lett. 61 (2007) 3432.
[18] K.R. Murali, J. Phys. Chem. Solid 68 (2007) 2293.
[19] Y. Kwon, Y. Li, Y.W. Heo, M. Jones, P.H. Hollyway, D.P. Norton, Z.V. Park, S. Li, Appl. Phys. Lett. 84 (2004) 2685.
[20] J.H. Lee, P. Lin, J.C. Ho, C.C. Lee, Electrochem. Solid-State Lett. 9 (2006) G117.
[21] K.C. Park, D.Y. Ma, K.H. Kim, Thin Solid Films 305 (1997) 201.
[22] B.D. Cullity, S.R. Stock, Elements of X-ray Diffraction, 2nd ed., Prentice-Hall, Inc, New Jersey, 2001, p. 388.
[23] G.W. Scherer, J. Sol–Gel Sci. Technol. 8 (1997) 353.
[24] R.D. Tarey, T.A. Raju, Thin Solid Films 128 (1985) 181.
[25] S.T. Tan, B.J. Chen, X.W. Sun, W.J. Fan, H.S. Kwok, X.H. Zhang, S.J. Chua, J. Appl. Phys. 98 (2005) 013505.